Supramolecular Host:Guest Arrays Site-Selectively Recognize Peptide Phosphorylation and Kinase Activity

Junyi Chen,[1] Parisa Fasihianifard,[1] Ria Lian,[1] Lucas J. Gibson-Elias,[1] Jose L. Moreno, Jr.,[1] Chia-En A. Chang,[1] Wenwan Zhong[2]* and Richard J. Hooley[1]*

[1]Department of Chemistry, University of California–Riverside, Riverside, CA 92521, U.S.A. [2]Key Laboratory of Precision and Intelligent Chemistry; Department of Chemistry, School of Chemistry and Materials Science; University of Science and Technology of China, Hefei, Anhui, 230026, P.R. China.

ABSTRACT: A synergistic combination of cationic styrylpyridinium dyes and water-soluble deep cavitand hosts can recognize phosphorylated peptides with both site- and state-selectivity. Two mechanisms of interaction are dominant: either the cationic dye interacts with Trp residues in the peptide or the host:dye pair forms a heteroternary complex with the peptide, driven by both strong dye-peptide and cavitand-peptide binding (K_d values up to 4 μM). The presence of multiple recognition mechanisms results in varying fluorescence responses dependent on phosphorylation state and position, eliminating the need for covalent modification of the peptide target. Differential sensing aided by machine learning algorithms permits full discrimination between differently positioned serine phosphorylations with a minimal 3-component array. The array is fully functional in the presence of Protein Kinase A (PKA) and its required cofactors, and capable of site-selective monitoring of serine phosphorylation at the privileged PKA motif, in the presence of serine residues that do not undergo reaction, illustrating the potential of the system in kinase-based drug screening.

Introduction

Phosphorylation is one of the most common and important post-translational modifications (PTMs), regulating protein functions and modulating signaling cascades.[1] Protein phosphorylation in cells is dynamic, responds promptly to diverse physiological stimuli, and tightly controlled by kinases and phosphatases.[2] Precise regulation of phosphorylation is delivered by phosphate writers and erasers, determined by both the type of amino acid and the localized sequence motif.[3] Dysregulation of these enzymes can cause pathological conditions, including inflammatory diseases, neurodegenerative diseases, cardiovascular diseases, and cancers.[4] Methods for phosphorylation site detection include mass-spectrometry-based proteomics,[5] the positional scanning peptide array (PSPA) method,[6] or nanopore sensors.[7] These methods, while powerful, require complex and expensive machinery, biosynthesis, and intricate sample preparation. High-throughput screening of kinase activity for revealing new drug candidates and improving therapeutic efficacy is commonly performed by detecting radio-isotopically labeled ATP.[8] While effective at revealing the state of phosphorylation, ATP-based detectors do not have *site selectivity*, a critical feature of kinases in precisely regulating signal transduction.

A multifaceted optical detection system that can selectively distinguish phosphorylated peptides while also monitoring kinase activity with site- and state-selectivity would be a valuable tool for deconvoluting signaling mechanisms and discovering novel therapeutic strategies. Fluorescence-based methods for phosphorylation detection are operationally simple, often using peptides covalently modified with a fluorophore.[9] Phosphorylation can modulate dye fluorescence via changing tyrosine-dye interaction, enhancing metal coordination, or inducing peptide-protein interaction. These sensors have also been applied to kinase and phosphatase sensing,[10] but are not functional on native peptides, and it is challenging to achieve site-selectivity. A solution lies in differential "chemical nose" sensors, which are powerful tools for the selective and sensitive detection of small changes in target structure.[11] These systems have been used to detect phosphorylation and kinase function with covalently modified peptides.[12] An extension of this concept is to exploit multiple synthetic hosts and indicator dyes that show variable non-covalent recognition of different targets, often by cavity-based molecular recognition of peptide modifications. The most popular targets are soft cations such as trimethyllysine (Kme_3) or methylated arginines, and excellent selectivity is possible.[13] The targets are also well-suited for supramolecular tandem assays of enzyme activity.[14]

We[15,16] and others[13,14] have exploited host:guest indicator arrays for the selective differentiation of peptide PTMs, and their application in monitoring chromatin writer and eraser activity, in some cases with site-selectivity.[16c] These systems are relatively simple in concept, in that the hosts can easily recognize soft cations such as the R-NMe_3^+ group and so the detection occurs via indicator displacement. However, other modifications (notably phosphate groups) are difficult targets for cavity-based recognition, so are challenging for indicator displacement systems.[17] As such, sensing peptide phosphorylation and kinase activity requires a different strategy.

We have previously shown that an "indirect" sensing mechanism can be exploited to detect peptide phosphorylation.[16d] In that case, the affinity between cationic peptide and an anionic receptor was the defining recognition characteristic: upon peptide phosphorylation, the overall charge of the target was changed, eliminating any affinity between host and peptide. In addition, a metal-assisted supramolecular tandem assay was applied to monitoring kinase/phosphatase activity. The challenge was that the sensor was only functional with highly cationic peptide strands, limiting scope, and no site-selectivity

was shown. More recently, we have discovered a new indirect sensing mechanism that is responsive to peptides containing a single tryptophan residue, and exploited this to selectively detect single isomers in peptide strands.[16e] Here, we combine these two indirect sensing concepts and show site- and state-selective recognition of peptide phosphorylation, as well as site-selective monitoring of kinase activity.

Results and Discussion

Detecting native peptide phosphorylation requires a judicious choice of target, one that shows sensitivity to the recognition system, but is also capable of reaction with a protein kinase. To this end, we focused on substrates for Protein Kinase A (PKA), as it is well-studied and robust. PKA is a central element in many of the regulatory processes in living cells, ubiquitously distributes in eukaryotic organisms and phosphorylates Ser or Thr at the specific phosphorylation site motif (R/K)-(R/K)-X-(Sp/Tp).[18] Our prior recognition system[16e] was selective for W-containing peptides, so a PKA substrate sequence (DDSRRWSDQLSLD) from the WD repeat and FYVE domain-containing protein 3 (Wdfy3) was selected. Wdfy3 is a key mediator for clearance of protein aggregates by autophagy, and its phosphorylation state is critical for its function.[19] This sequence contains multiple possible phosphorylation sites: serine 7 (S7) corresponds to the PKA phosphorylation motif. Wdfy3 variants with phosphorylation at either S3, S7 or both S3 and S7 were synthesized for testing, as well as the unmodified peptide (Figure 1).

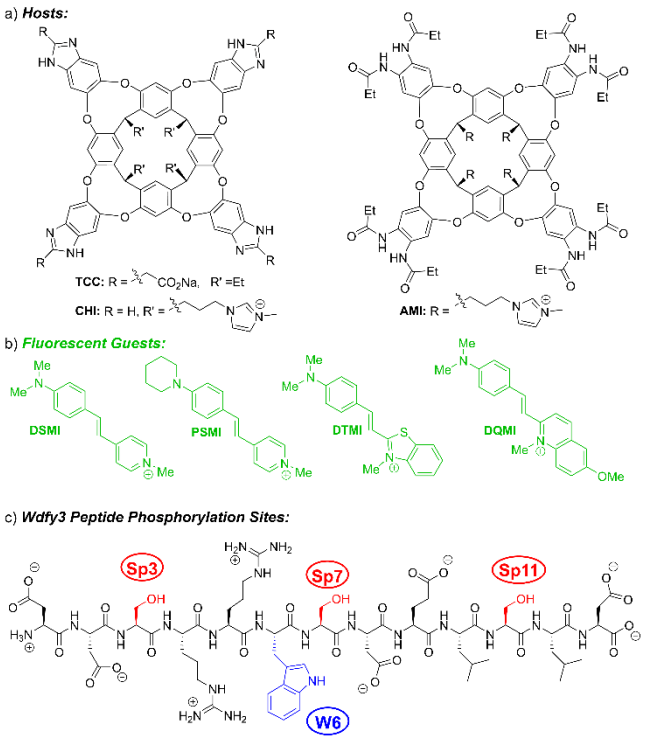

Figure 1. The structures of a) cavitands and b) dyes, c) the sequence of Wdfy3 peptides used in this study.

The recognition system consists of an arrayed combination of water-soluble deep cavitands and styrylpyridinium indicator dyes (Figure 1). These arrays can exploit an indirect recognition mechanism whereby the cationic, hydrophobic dye binds W-containing peptides *via* π-stacking interactions.[16e] Competitive recognition of the dye by different deep cavitands confers multiple equilibria on the system, causing variable dye emission in each array element, which is vital for differential sensing. Because the wild-type (WT) sequence of Wdfy3 has a theoretical pI of 3.87 and shows a net charge of -2.0 at neutral pH, along with the presence of Trp at position 6, it is a viable candidate for selective recognition by the dye:host system, and variable serine phosphorylations should affect the affinity and response. To test this hypothesis, a series of dyes and host cavitands were combined, and their emission response with the Wdfy3 peptides was analyzed. The host cavitands **TCC**, **CHI** and **AMI**, and styrylpyridinium dyes **DSMI**, **PSMI**, **DTMI** and **DQMI** have all shown efficacy as differential sensors,[15] so were chosen as the initial sensing elements. As the hypothesis was that the dyes would show response to the W-containing peptide, these were tested first.

Three Wdfy3 variants (WT, Sp3 and Sp7, 0–10 μM) were titrated into a solution of dye (either **DSMI**, **PSMI**, **DTMI** or **DQMI**, 0.5 μM in 20 mM Tris buffer, pH 7.4) and the fluorescence response measured. Two of the plots are shown in Figure 2a-b (for the full data set, see Figures S-5 and S-6). In each case, the fluorescence intensity of the dyes is enhanced in the presence of peptide, but the enhancement varies between the wild-type and phosphorylated variants. Most notably, the Sp7 peptide shows a much lower emission enhancement for each of the dyes than the unphosphorylated parent. In contrast, the response for Sp3 is quite similar (but not identical) to that for the wild-type strand, in particular for low [peptide]. This variable emission enhancement suggests that the dyes are indeed binding the peptide as hypothesized. Further evidence for the dye:peptide interaction was obtained by monitoring the intrinsic tryptophan fluorescence of the Wdfy3 peptide upon addition of dye. Trp residues exhibit emission at 350 nm when excited at 280 nm:[20] the quantum yield is sensitive to the local electrostatic environment, and the fluorescence can be easily quenched upon addition of ligand. Titration of the 4 dyes into a 4 μM solution of WT Wdfy3 caused variable Trp quenching (Figure 2c), corroborating the prior results.

Molecular Dynamics (MD) simulations were performed for the association of **DTMI** and three Wdfy3 variants (WT, Sp3, Sp7) in a water box using the AMBER20 simulation package with ff14sb force field.[21] The trajectories of 500ns MD runs were analyzed, and the interaction energies between the dye and various conformations of Wdfy3 were calculated using the molecular mechanics/Poisson-Boltzmann surface area (MM/PBSA) method. This allowed determination of the relative interaction energies between the dye and different conformations of Wdfy3. The MD analysis revealed a spectrum of complex conformations, highlighting that **DTMI** can bind to multiple sites with different affinities. The structures of the most favorable interactions are shown in Figure 2. These optimized structures provide a hint as to why the dyes are differentially selective for the Wdfy3 peptide. The **DTMI**•WT Wdfy3 complex (Figure 2d) shows that the most favorable conformation obtained positions the dye in proximity with Trp-6, showing π-stacking interactions with the sidechain, as well as cation- π interactions with a nearby Arg residue. All 3 serines (at positions 3, 7 and 11) are close enough to the bound dye for phosphorylation to affect the recognition. Indeed, the results of modeling **DTMI** with the two variants show different peptide conformations that retain the **DTMI**-Trp 6 interaction. The most notable differences are that the phosphate group in Sp3 is oriented away from the bound dye, whereas the phosphate in Sp7 is in close proximity to it: the binding can still occur, but the presence of the phosphates has differential effects based on position. Notably,

the dye fluorescence responses for WT and Sp3 (which shows a remotely oriented phosphate) are quite similar, and Sp7 (with a phosphate closer to the dye upon binding) shows far lower response (see Figure 2a).

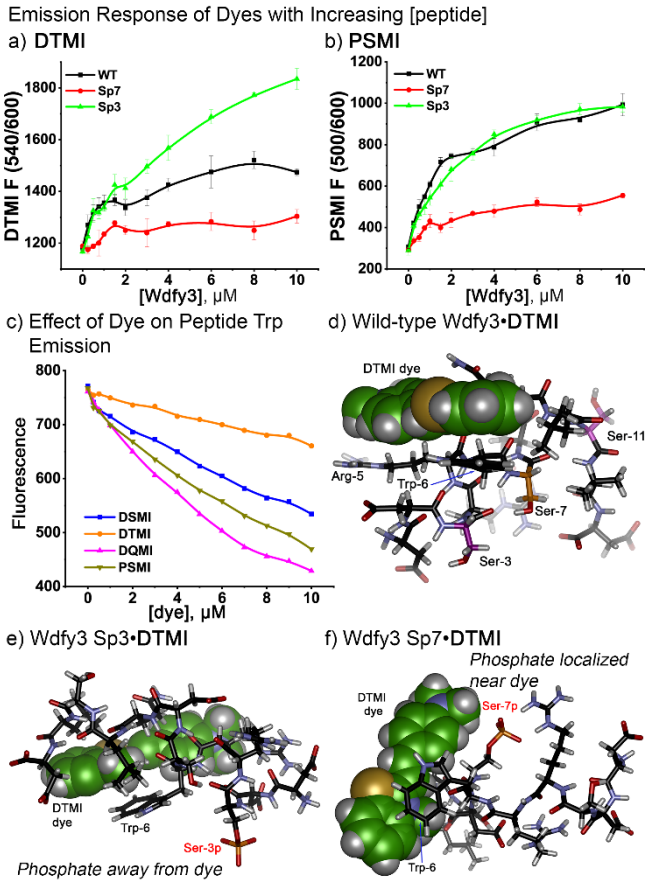

Figure 2. Dye:Peptide Complex Formation. Plots of dye fluorescence emission changes at optimal Ex/Em wavelengths Wdfy3-dye titration curves upon titration of 0 – 10 μM Wdfy3 to a) 0.5 μM **DTMI**; b) 0.5 μM **PSMI**, c) Tryptophan emission changes upon titration of 0-10 μM dye to 4μM WT Wdfy3 (20 mM Tris, pH = 7.4). Optimized structures determined by molecular dynamics simulation of **DTMI** and Wdfy3 peptides: d) wild-type (WT), e) Sp3, and f) Sp7.

While the dyes show differential affinity for the Wdfy3 variants, they are not capable of fully distinguishing the variants by themselves (see Figures S-21 and S-22 for discriminant analysis plots). The selectivity can be enhanced by adding a second element, water-soluble deep cavitands. As the **TCC/CHI/AMI** cavitands have been shown to be competitive receptors for the styrylpyridinium dyes,[15] the effect of cavitand on the dye:peptide response was tested. The fluorescence response of various Wdfy3 peptides (4 μM in 20 mM Tris buffer, pH 7.4) to a combination of 0.5 μM dye and cavitand (**TCC**, **AMI**, or **CHI**) at varying concentrations up to 16 μM) was measured, as can be seen in Figures 3c–e and Figures S7 – S14. The initial concept was that the hosts would simply compete with the peptide for dye binding: as the different dyes have variable affinity for both different peptides and different cavitands, they can constitute the arrays for differential sensing. However, while the emission of the dye-cavitand complex is much higher than that of the dye-peptide complex, the emission profiles of the different cavitand:dye combinations in the presence of Wdfy3 peptides were highly variable, and in some cases the fluorescence of the cavitand:dye:peptide mixture was higher than that of the cavitand:dye complex. These results indicate that the cavitand hosts were not simply competitive receptors for the dyes, but also interacted with the Wdfy3 peptide. This effect has been seen for the anionic **TCC** host with cationic Histone H3 peptides,[16d] but was unexpected for these anionic Wdfy3 strands. As such, we analyzed the affinity of Wdfy3 for the three cavitands by monitoring the change in Trp fluorescence upon titration of cavitand (Figure 3b). The affinity of the cavitand hosts to the WT Wdfy3 was generally similar to that of the dye:peptide affinity, with K_d (cavitand:Wdfy3) = 6 – 21 μM and K_d (dye:Wdfy3) = 4 – 47 μM. In addition, the cavitand:dye affinities are in a similar range, varying from K_d = 2 – 135 μM (see Supporting Table S-2 for full data).

The variable affinity profiles allow a better understanding of the emission profiles of the different cavitand:dye combinations in the presence of Wdfy3 peptides. The emission curves represent the sum of all the interactions occurring between peptide, cavitand and dye in each mixture, so deconvoluting them to identify all major contributors is challenging. There are however, certain trends that can be gleaned from the responses, and these trends can be separated into three broadly defined groups (illustrated in Figure 3a). Group 1) is a simple competitive binding mechanism, which is dominant for the **DSMI** dye (with all cavitands), and the **TCC** cavitand (with all 4 dyes, see Figures S-7, S-9a, S-11a, and S-13a). In this case, the emission increase upon formation of a cavitand:dye complex vastly outweighs the emission increase from peptide:dye complexation – the relative affinities of cavitand:dye and peptide:dye are the dominant factors that control the emission profile. Group 2) is seen with the cationic **AMI** cavitand, which has the lowest affinity for the dyes and the highest affinity for peptide. Upon titration of **AMI** into a solution of Wdfy3 variants and dye (4 μM peptide, 0.5 μM dye in 20 mM Tris buffer, pH 7.4), there is a sharp spike in emission at low [**AMI**] (<2 μM), followed by a plateau at higher [**AMI**] (see Figures 3c, d and Figures S-9c, S-11c, S-13c). This is indicative of the formation of a cavitand:dye:peptide ternary complex, and the emission is highly dependent on the phosphorylation state of the peptide. The **AMI** host gives rise to the most variable emission curves, especially at low [**AMI**]. Evidently multiple complexes are possible, including different peptide:dye conformations, as well as cavitand:dye and ternary complexes. The lower **AMI** affinity for the dyes allows these multiple different complexes to be present in noticeable concentrations, which elevates the complexity of the emission profiles. Importantly, the major takeaway is that the initial sharp emission increase followed by a plateau is most reasonably explained by ternary complex formation. Group 3) lies in-between the two prior states, and involves the cationic cavitand **CHI**. As can be seen most notably when combined with **PSMI** (Figure 3e), dye emission is enhanced with increasing [**CHI**], but the increase is not linear, suggesting that both the ternary complex formation and competitive recognition processes are occurring, and neither one is dominant.

The main takeaway from this data is that the sensing elements are dependent on multiple binding equilibria, as well as the nature of the dye and cavitand used. The relative affinities of cavitand:dye and peptide:dye determine the emission, and can take advantage of ternary complexes between peptide, cavitand and dye, rather than just competitive recognition. The affinity titrations (vide supra) were used to select the most favorable dye:cavitand ratios, focusing on those that gave the greatest difference between the three tested Wdfy3 peptides (WT, Sp3 and Sp7), i.e. dye:cavitand ratios of 0.5:2

or 0.5:4, with the exception being **TCC**, which favored a 0.5:0.5 ratio. This initial 25-element array was applied to sense the various Wdfy3 peptides (see Figures S19 – S20 for the full dataset). The data was subjected to support vector machine (SVM)-recursive feature elimination with cross-validation (RFECV) to narrow the scope and determine the array constituents that were most effective in peptide discrimination. SVM-RFECV is a classic machine learning algorithm for optimal feature selection,[22] which we have previously used for choosing sensor elements for biomarker classification.[23]

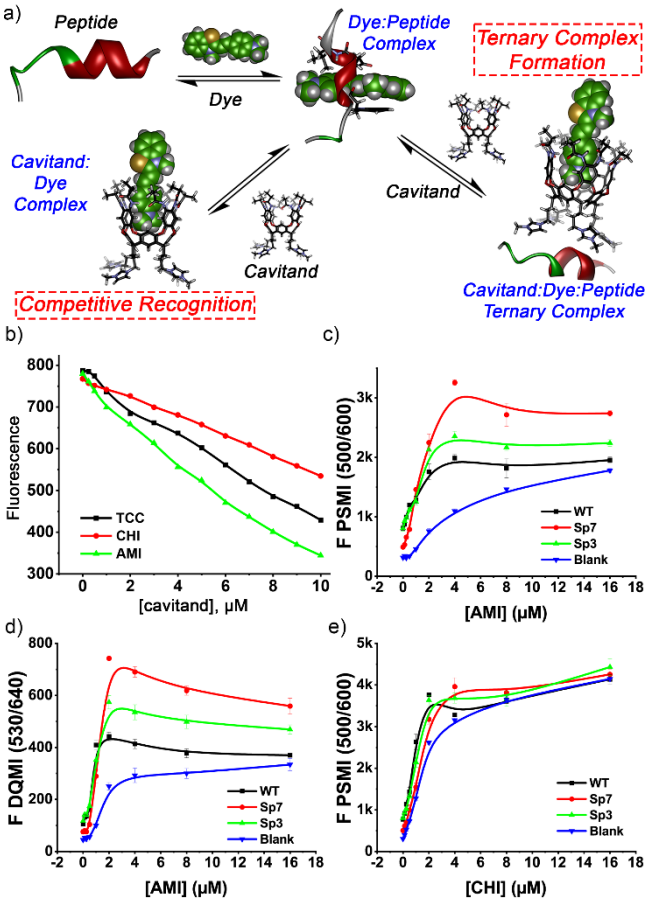

Figure 3. Recognition Mechanisms. a) Illustration of the various complexes formed by the host, dye and peptide combinations. b) Tryptophan emission upon titration of 0 – 10 μM cavitand to 4μM WT Wdfy3 (20 mM Tris, pH = 7.4). Plots of dye fluorescence emission changes at optimal Ex/Em wavelengths upon titration of cavitand into a dye:peptide mixture: c) **AMI** into **PSMI** + peptide; d) **AMI** into **DQMI** + peptide; e) **CHI** into **PSMI** + peptide ([dye] = 0.5 μM, [peptide] = 4 μM, 20 mM Tris buffer, pH at 7.4).

To ensure that the array was fully functional in all cases, including kinase sensing, we selected a medium-sized array using the top 8 elements found by SVM-RFECV: **DSMI•0.5TCC**, **DSMI•4AMI**, **DTMI•4AMI**, **DTMI•2CHI**, **DQMI•2AMI**, **DQMI**, **PSMI•2CHI**, and **PSMI•2AMI**, where "**2AMI**", etc. refers to the concentration of cavitand used (2 μM in that case). The fluorescence responses to these 8 elements are shown in Figure 4a, which illustrates the wide range of responses for the different elements. While it is challenging for PCA (Figure S-28) to distinguish all 4 targets, a 2D t-SNE plot (Figure 4b) shows that the medium-sized 8-element sensing array was able to differentiate all four peptides. In contrast to PCA which is a linear dimensionality reduction algorithm that concentrates on placing data points far apart,[11b] t-SNE is a nonlinear unsupervised dimensionality reduction technique that not only retains maximum variance but also preserves the relationship between data points in a lower dimensional space.[24] Even so, there is a small overlap between WT and Sp3 in the t-SNE plot. Sp7 and Sp3Sp7 can be well separated from WT and Sp3, however: this mirrors the results from dye:peptide modeling, where the Sp3 phosphorylation was remote from the dye, and the difference with WT was small, whereas the phosphorylation in Sp7 was closer to the bound dye.

The advantage of array sensing is that while certain sensor elements could be optimal for different tasks (i.e. differentiating the phosphorylation state or site), when combined they can provide full discrimination of all targets. Therefore, to reveal the contribution of each sensor in state- and site-selectivity, starting from a full array, we applied the SVM-RFECV algorithm to multiple tasks, focusing on: 1) determining *state*-selectivity, i.e. differentiating between 0 (WT), 1 (Sp3 or Sp7) or 2 (Sp3Sp7) serine phosphorylations on the Wdfy3 sequence; 2) determining *site*-selectivity, i.e. discriminating between Sp3 and Sp7; and 3) discriminating the full suite of peptides WT, Sp3, Sp7 and Sp3Sp7. Only 2 elements are needed to allow full state-selectivity: in this case, the peptides are treated as 3 targets, with zero (WT), one (Sp3 and Sp7) or two (Sp3Sp7) phosphorylations, and using only **DTMI•4AMI** and **PSMI•2CHI** confers full separation (see Figure S-29). On the other hand, if only two peptides are analyzed for site-selectivity (Sp3 and Sp7), full discrimination is possible with a single element **DSMI•0.5TCC** in 1D t-distribution curve (see Figure S-30).

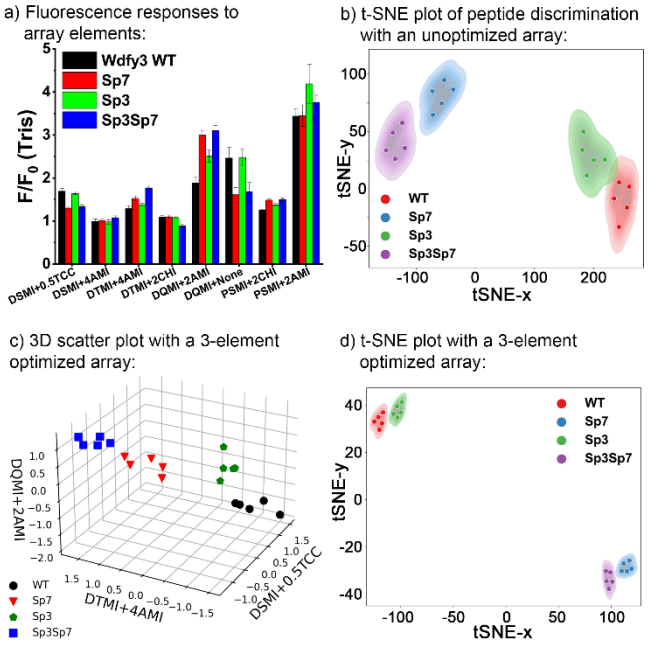

Figure 4. a) The bar plot and b) t-SNE plot of the fluorescence responses of the initial 8-element array to the four Wdfy3 variants. c) 3D scatter plot using scaled F/F_0 and d) the t-SNE plot of the fluorescence responses of the top 3 array elements for discriminating WT vs Sp7 vs Sp3 vs Sp3Sp7. [peptide] = 4 μM, [dye] = 0.5 μM, [cavitand] = 0.5/2/4 μM, depending on array element, 20 mM Tris buffer, pH at 7.4).

For discriminating the full suite of peptides, SVM-RFECV suggested three elements were sufficient: **DTMI•4AMI**, **DQMI•2AMI**

and **DSMI•0.5TCC**. Figures 4c and 4d show two processing outputs for the data, a 3D scatter plot and a 2D t-SNE plot, respectively. The 3D scatter plot clearly shows the contribution of the three top elements to the discrimination tasks. **DSMI•0.5TCC** is effective at separating the Sp7-containing peptide from WT and Sp3, **DQMI•2AMI** can separate WT and Sp3, and **DTMI•4AMI** is key for differentiating Sp7 and Sp3Sp7. Full separation is observed with t-SNE, illustrating the effectiveness of SVM-RFECV in selecting the optimal elements for discrimination. Notably, while the dyes themselves are effective at distinguishing the unmodified peptide from Sp7, the more challenging discriminations requires the cavitand:dye combination, illustrating the importance of the cavitand:dye:peptide ternary complexes for site-selectivity.

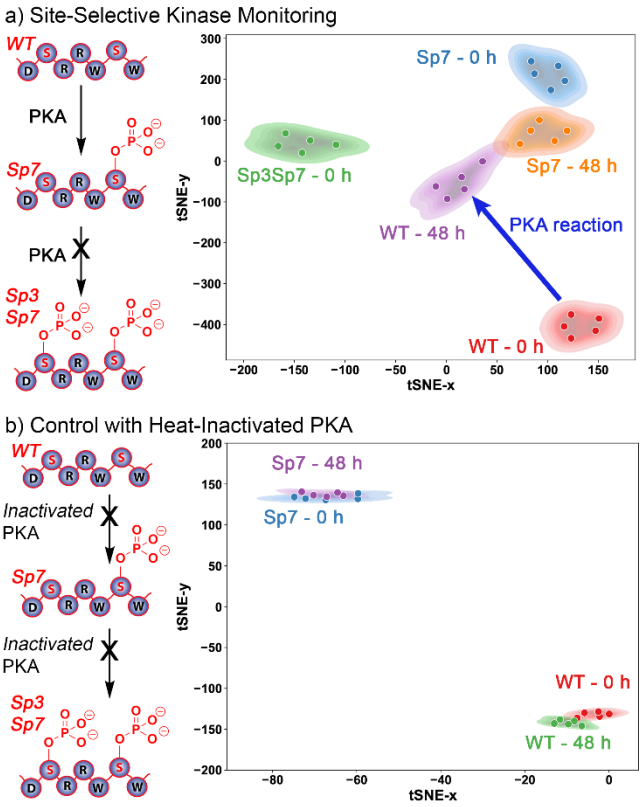

Figure 5. Site-Selective Kinase Sensing. a) t-SNE plot from F/F_0 data of the PKA reaction with various Wdfy3 peptides using the optimal 3-element array; b) t-SNE plot from F/F_0 data of the reaction of peptides with inactivated PKA using the initial 8 element array. 0.002 mg/mL PKA, 20 mM Tris, 40 μM ATP, 0.2mM $MgCl_2$, 0.4 μM cAMP, [peptide] = 4 μM, [dye] = 0.5 μM, [cavitand] = 0.5/2/4 μM, depending on array element.

As the minimal array is highly effective in discriminating the various phosphopeptides, it should be well-suited for site-selective kinase monitoring, but this introduces a second challenge: tolerance to the PKA reaction mixture. The sensor elements must be tolerant to the enzyme, cofactors and media, as well as retaining selectivity and sensitivity for the target phosphopeptides. To that end, the Wdfy3 peptides WT, Sp3, Sp7 and Sp3Sp7 were subjected to the initial 8-element sensing array in the presence of PKA enzyme in the reaction buffer (0.002 mg/mL PKA, 20 mM Tris, 40 μM ATP, 0.2 mM $MgCl_2$, 0.4 μM cAMP, the necessary components for the PKA reaction).[25] The measurements were taken immediately (0 h), to ensure no reaction had taken place. As can be seen in Figure S-32a and S-33, this array was fully capable of discriminating the 4 peptides in the reaction conditions. The top 3 elements selected by SVM-RFECV (**DSMI•0.5TCC**, **DTMI•4AMI**, **DQMI•4AMI**, Figure S-34) are identical to those obtained as optimal for sensing the 4 peptides in Tris buffer, illustrating the tolerance of the array to the complex enzyme reaction mixture.

Finally, we focused on applying the array for site- and state-selective sensing of the PKA-catalyzed phosphorylation of Wdfy3. Each of the 4 peptides Wdfy3 (WT, pS7, pS3, Sp3Sp7) were subjected to the same PKA reaction conditions (vide supra), and the reaction monitored over time. Aliquots were taken, and subjected to matrix-assisted laser desorption/ionization (MALDI) mass spectrometry to determine reaction progress (obviously without site-selectivity, but this method could verify whether the peptide was converted into the corresponding phosphate or not). The MALDI analysis showed that the reaction of WT Wdfy3 was >70% complete after 48 h, whereas Sp7 and Sp3Sp7 were unreacted (as expected). The Sp3 peptide, which contains a free serine at position 7 (the reactive PKA motif) did undergo some phosphorylation, albeit substantially less than WT, with only ~22% conversion after 48 h.

The reaction aliquots were also added to the 8-element array, and the fluorescence responses analyzed, comparing the fluorescence responses after 0 h and 48 h (see Figure S-32 for full data). The responses of the top 3 elements (as described above) were subjected to t-SNE, and the resulting plot is shown in Figure 5a. This plot clearly shows the movement of the signals for WT Wdfy3 upon reaction – before the PKA process, the signals for WT-0h (red) are clustered far away from the other initial peptides Sp7 (blue) and Sp3Sp7 (green). Upon reaction, the product signals for WT-48h (purple) are closely located by those of the Sp7 product, remote from the Sp3Sp7 signals, indicating that the array was capable of not only detecting phosphorylation, but that the phosphorylation occurred at Ser 7 (rather than Ser 3). The Sp7 signals moved only slightly after 48 h reaction, indicating no reaction (as expected) with PKA. The sensor output was also compared to that of the unreacted Wdfy3 Sp3 and Sp3Sp7, whereby the Sp3 peptide was spiked into the non-peptide reaction mixture and heated in the same manner as the real enzyme reaction. The t-SNE plot (see Figure S-37) shows that the product is located near the position of Sp7, but far from Sp3 and Sp3Sp7, reinforcing both the site- and state-selectivity of the system.

Further evidence for the performance of the sensor is shown in Figure 5b, whereby the process was repeated with a heat-inactivated enzyme. The PKA enzyme was heated in boiling water for 30 minutes, then sonicated for 30 minutes and vortexed to allow redissolution. Both WT and Sp7 Wdfy3 were subjected to "reaction" with this inactivated enzyme, using identical conditions to the prior process with active PKA. Figure 5b shows the t-SNE plot of the fluorescence responses for WT and Sp7 both before and after exposure to the inactivated reaction conditions, and clearly show minimal movement in the t-SNE plot in each case: the array can accurately report the outcomes of both successful and failed reaction, and the sensing components are tolerant to the enzymatic reaction conditions.

The performance of the sensor array is impressive: in the presence of multiple different phosphate-containing species (ATP, cAMP), enzyme and salt, a 3-component sensor is able to monitor the site-selective phosphorylation of a native peptide solely via non-covalent molecular recognition. Perhaps most impressively, the sensor was

able to function in mixtures of peptides, as the enzyme reaction was not complete under the conditions after 48h, only converting 70% WT peptide to Sp7, and yet this imperfect reaction could still be monitored. However, there were some limitations – while the array performed well for high-yielding enzymatic transformations (of WT), it was challenging to accurately analyze low-yielding reactions. The low-yielding conversion of Sp3 to Sp3Sp7 required the 8-element array to detect, and this showed the product mixture moving towards (but obviously not overlapping) the Sp3Sp7 product in the t-SNE plot (see Figure S-35). This is understandable, but an area we will focus on improving in the future. In addition, the best performance in kinase sensing required aliquots to be taken from the reaction mixture: when the reaction was performed in the presence of the array components (notably the **TCC** cavitand), some interference with the kinase reaction was seen. However, the sensor was able to accurately track a reaction progress mimic, monitoring manually varied concentrations of Wdfy3 WT vs Sp7 in the absence of enzyme but in the presence of all the other reaction components (Figures S23 – 25). This illustrates the future potential of the system as an *in-situ* site-selective kinase assay.

Conclusions

Here, we have shown that a combination of cationic dyes and water-soluble deep cavitands can be applied for indirect sensing of native, unmodified peptides and their phosphorylation state. By exploiting multiple recognition mechanisms, site-selectivity in phosphorylation detection can be achieved: the dyes can interact with Trp residues in the peptide, and the host:dye conjugates can form ternary complexes with the target. Molecular modeling suggests that the peptide folds around the dye target, and this interaction is dependent on phosphorylation state and site, conferring selectivity on the process. By adding a second element, deep cavitands, competitive equilibria are introduced, either simple competitive recognition of the dye or formation of host:dye:peptide ternary complexes. Differential sensing allows full discrimination between peptide targets, and machine learning can be exploited to reveal the key sensors for site- or state-selectivity, and create a minimal array of only 3 components. This array is fully functional in the presence of PKA and its cofactors, allowing site-selective monitoring of serine phosphorylation – mostly notably, the indirect nature of the recognition allows the sensor to be selective in the presence of other phosphorylated species, notably ATP and cAMP. This selectivity is reminiscent of that of antibodies, but uses a simple synthetic host:guest system with native peptide substrates for highly complex molecular recognition.

ASSOCIATED CONTENT

Supporting Information

Fluorescence data, molecular dynamics analysis, and statistical methods. This material is available free of charge via the Internet at http://pubs.acs.org.

AUTHOR INFORMATION

Corresponding Author

* E-mail: richard.hooley@ucr.edu; wenwanz@ustc.edu.cn.

ACKNOWLEDGMENTS

The authors would like to thank the National Science Foundation (CHE-2305089 to R.J.H. and MCB-1932984 to C-E.A.C., as well as CHE-1828782 for an AB-SCIEX 5800 MALDI TOF/TOF System) for funding, and the University of Science and Technology of China (to W.Z.) for support. The authors would like to thank Liyi Chen and Xin Wen for suggestions on data analysis.

REFERENCES

(1) (a) Bah, A.; Vernon, R. M.; Siddiqui, Z.; Krzeminski, M.; Muhandiram, R.; Zhao, C.; Sonenberg, N.; Kay, L. E.; Forman-Kay, J. D. Folding of an Intrinsically Disordered Protein by Phosphorylation as a Regulatory Switch. *Nature* **2015**, *519*, 106–109. (b) Gough, N. R.; Foley, J. F. Focus Issue: Systems Analysis of Protein Phosphorylation. *Sci. Signal.* **2010**, *3*, eg6. (c) Guo, X.; Wang, X.; Wang, Z.; Banerjee, S.; Yang, J.; Huang, L.; Dixon, J. E. Site-specific Proteasome Phosphorylation Controls Cell Proliferation and Tumorigenesis. *Nat. Cell Biol.* **2016**, *18*, 202–212. (d) Humphrey, S. J.; Azimifar, S. B.; Mann, M. High-Throughput Phosphoproteomics Reveals *in vivo* Insulin Signaling Dynamics. *Nat. Biotechnol.* **2015**, *33*, 990–995.

(2) (a) Caenepeel, S.; Charydczak, G; Sudarsanam, S; Hunter, T.; Manning, G. The Mouse Kinome: Discovery and Comparative Genomics of All Mouse Protein Kinases. *Proc. Natl. Acad. Sci. USA.* **2004**, *101*, 11707–11712. (b) Manning, G; Whyte, D.B.; Martinez, R., Hunter, T., Sudarsanam, S. The Protein Kinase Complement of the Human Genome. *Science* **2002**, *298*, 1912–1934. (c) Köhn, M. Turn and Face the Strange: A New View on Phosphatases. *ACS Cent. Sci.* **2020**, *6*, 467–477.

(3) (a) Yaron-Barir, T. M.; Joughin, B. A.; Huntsman, E. M.; Kerelsky, A.; Cizin, D. M.; Cohen, B. M.; Regev, A.; Song, J.; Vasan, N.; Lin, T.-Y.; Orozco, J. M.; Schoenherr, C.; Sagum, C.; Bedford, M. T.; Wynn, R. M.; Tso, S.-C.; Chuang, D. T.; Li, L.; Li, S. S. C.; Creixell, P.; Krismer, K.; Takegami, M.; Lee, H.; Zhang, B.; Lu, J.; Cossentino, I.; Landry, S. D.; Uduman, M.; Blenis, J.; Elemento, O.; Frame, M. C.; Hornbeck, P. V.; Cantley, L. C.; Turk, B. E.; Yaffe, M. B.; Johnson, J. L. The Intrinsic Substrate Specificity of the Human Tyrosine Kinome. *Nature* **2024**, *629*, 1174–1181. (b) Yaffe, M. B.; Leparc, G. G.; Lai, J.; Obata, T.; Volinia, S.; Cantley, L. C. A Motif-Based Profile Scanning Approach for Genome-Wide Prediction of Signaling Pathways. *Nat. Biotechnol.* **2001**, *19*, 348–353.

(4) (a) Ferguson, F. M.; Gray, N. S. Kinase Inhibitors: the Road Ahead. *Nat. Rev. Drug Discov.* **2018**, 17, 353–377. (b) Cohen, P.; Cross, D.; Jänne, P. A. Kinase Drug Discovery 20 years After Imatinib: Progress and Future Directions. *Nat. Rev. Drug Discov.* **2021**, *20*, 551–569. (c) Blume-Jensen, P.; Hunter, T. Oncogenic Kinase Signalling. *Nature* **2001**, *411*, 355–365. (d) Castelo-Soccio, L.; Kim, H.; Gadina, M.; Schwartzberg, P. L.; Laurence, A.; O'Shea, J. J. Protein Kinases: Drug Targets for Immunological Disorders. *Nat. Rev. Immunol.* **2023**, *23*, 787–806. (e) Attwood, M. M.; Fabbro, D.; Sokolov, A. V.; Knapp, S.; Schiöth, H. B. Trends in Kinase Drug Discovery: Targets, Indications and Inhibitor Design. *Nat. Rev. Drug Discov.* **2021**, *20*, 839–861.

(5) (a) Mann, M.; Jensen, O. N. Proteomic Analysis of Post-translational Modifications. *Nat. Biotechnol.* **2003**, *21*, 255–261. (b) Conibear, A. C. Deciphering Protein Post-Translational Modifications Using Chemical Biology Tools. *Nat. Rev. Chem.* **2020**, *4*, 674–695.

(6) Johnson, J. L.; Yaron, T. M.; Huntsman, E. M.; Kerelsky, A.; Song, J.; Regev, A.; Lin, T.-Y.; Liberatore, K.; Cizin, D. M.; Cohen, B. M.; Vasan, N.; Ma, Y.; Krismer, K.; Robles, J. T.; van de Kooij, B.; van Vlimmeren, A. E.; Andrée-Busch, N.; Käufer, N. F.; Dorovkov, M. V.; Ryazanov, A. G.; Takagi, Y.; Kastenhuber, E. R.; Goncalves, M. D.; Hopkins, B. D.; Elemento, O.; Taatjes, D. J.; Maucuer, A.; Yamashita, A.; Degterev, A.; Uduman, M.; Lu, J.; Landry, S. D.; Zhang, B.; Cossentino, I.; Linding, R.; Blenis, J.; Hornbeck, P. V.; Turk, B. E.; Yaffe, M. B.; Cantley, L. C. An Atlas of Substrate Specificities for the Human Serine/Threonine Kinome. *Nature* **2023**, *613*, 759–766.

(7) (a) Martin-Baniandres, P.; Lan, W.-H.; Board, S.; Romero-Ruiz, M.; Garcia-Manyes, S.; Qing, Y.; Bayley, H. Enzyme-Less Nanopore Detection of Post-Translational Modifications within Long Polypeptides. *Nat. Nanotechnol.* **2023**, *18*, 1335–1340. (b)Lan, W.-H.; He, H.; Bayley, H.; Qing, Y. Location of Phosphorylation Sites within Long Polypeptide Chains by Binder-Assisted Nanopore Detection. *J. Am. Chem. Soc.* **2024**, *146*, 24265–24170.

(8) (a) Anastassiadis, T.; Deacon, S. W.; Devarajan, K.; Ma, H.; Peterson, J. R. Comprehensive Assay of Kinase Catalytic Activity Reveals Features of Kinase Inhibitor Selectivity. *Nat. Biotechnol.* **2011**, *29*, 1039–1045. (b) Hastie, C. J.; McLauchlan, H. J.; Cohen, P. Assay of Protein Kinases Using Radiolabeled ATP: A Protocol. *Nat. Protoc.* **2006**, *1*, 968–971.

(9) (a) Li, M.; Xiong, Y.; Qing, G. Innovative Chemical Tools to Address Analytical Challenges of Protein Phosphorylation and Glycosylation. *Acc. Chem. Res.* **2023**, *56*, 2514–2525. (b) Hu, J.; Gao, L. Recent Advances in Fluorescent Chemosensors for Protein Kinases. *Chem. Asian J.* **2022**, 17, e202200182. (c) Macreadie, L. K.; Gilchrist, A. M.; McNaughton, D. A.; Ryder, W. G.; Fares, M.; Gale, P. A. Progress in Anion Receptor Chemistry, *Chem* **2022**, *8*, 46–118. (d) González-Vera, J. A. Probing the Kinome in Real Time with Fluorescent Peptides. *Chem. Soc. Rev.* **2012**, *41*, 1652–1664. (e) H. S. Lu, C.; Liu, K.; Tan, L. P.; Yao, S. Q. Current Chemical Biology Tools for Studying Protein Phosphorylation and Dephosphorylation. *Chem.-Eur. J.* **2012**, *18*, 28–39.

(10) (a) Lawrence, D. S.; Wang, Q. Seeing is Believing: Peptide-Based Fluorescent Sensors of Protein Tyrosine Kinase Activity. *Chembiochem* **2007**, *8*, 373–378. (b) Shults, M. D.; Imperiali, B. Versatile Fluorescence Probes of Protein Kinase Activity. *J. Am. Chem. Soc.* **2003**, *125*, 14248–14249. (c) Chen, C.-A.; Yeh, R.-H.; Lawrence, D. S. Design and Synthesis of a Fluorescent Reporter of Protein Kinase Activity. *J. Am. Chem. Soc.* **2002**, *124*, 3840–3841. (d) Sahoo, H.; Hennig, A.; Florea, M.; Roth, D.; Enderle, T.; Nau, W. M. Single-Label Kinase and Phosphatase Assays for Tyrosine Phosphorylation Using Nanosecond Time-Resolved Fluorescence Detection. *J. Am. Chem. Soc.* **2007**, *129*, 15927–15934. (e) Anai, T.; Nakata, E.; Koshi, Y.; Ojida, A.; Hamachi, I. Design of a Hybrid Biosensor for Enhanced Phosphopeptide Recognition Based on a Phosphoprotein Binding Domain Coupled with a Fluorescent Chemosensor. *J. Am. Chem. Soc.* **2007**, *129*, 6232–6239. (f) Turner, A. H.; Lebhar, M. S.; Proctor, A.; Wang, Q.; Lawrence, D. S.; Allbritton, N. L. Rational Design of a Dephosphorylation-Resistant Reporter Enables Single-Cell Measurement of Tyrosine Kinase Activity. *ACS Chem. Biol.* **2016**, *11*, 355–362. (g) O'Banion, C. P.; Priestman, M. A.; Hughes, R. M.; Herring, L. E.; Capuzzi, S. J.; Lawrence, D. S. Design and Profiling of a Subcellular Targeted Optogenetic cAMP-Dependent Protein Kinase. *Cell Chem. Biol.* **2018**, *25*, 100–109. (h) Wells, C. I.; Drewry, D. H.; Pickett, J. E.; Tjaden, A.; Krämer, A.; Müller, S.; Gyenis, L.; Menyhart, D.; Litchfield, D. W.; Knapp, S.; Axtman, A. D. Development of a Potent and Selective Chemical Probe for the Pleiotropic Kinase CK2. *Cell Chem. Biol.* **2021**, *28*, 546–558. (i) Oien, N. P.; Nguyen, L. T.; Jernigan, F. E.; Priestman, M. A.; Lawrence, D. S. Long-Wavelength Fluorescent Reporters for Monitoring Protein Kinase Activity. *Angew. Chem. Int. Ed.* **2014**, *53*, 3975–3978. (j) Luković, E.; González-Vera, J. A.; Imperiali, B. Recognition-Domain Focused Chemosensors: Versatile and Efficient Reporters of Protein Kinase Activity. *J. Am. Chem. Soc.* **2008**, *130*, 12821–12827.

(11) (a) You, L.; Zha, D.; Anslyn, E.V. Recent Advances in Supramolecular Analytical Chemistry Using Optical Sensing. *Chem. Rev.* **2015**, *115*, 7840–7892. (b) Stewart, S.; Ivy, M. A.; Anslyn, E. V. The Use of Principal Component Analysis and Discriminant Analysis in Differential Sensing Routines. *Chem. Soc. Rev.* **2014**, *43*, 70–84. (c) Sedgwick, A. C.; Brewster, J. T.; Wu, T.; Feng, X.; Bull, S. D.; Qian, X.; Sessler, J. L.; James, T. D.; Anslyn, E. V.; Sun, X. Indicator Displacement Assays (IDAs): the Past, Present and Future. *Chem. Soc. Rev.* **2021**, *50*, 9–38. (d) Pinalli, R.; Pedrini, A.; Dalcanale, E. Biochemical Sensing with Macrocyclic Receptors. *Chem. Soc. Rev.* **2018**, *47*, 7006–7026. (e) van Dun, S.; Ottmann, C.; Milroy, L.-G.; Brunsveld, L. Supramolecular Chemistry Targeting Proteins. *J. Am. Chem. Soc.* **2017**, *139*, 13960–13968. (f) Krämer, J.; Kang, R.; Grimm, L. M.; De Cola, L.; Picchetti, P.; Biedermann, F. Molecular Probes, Chemosensors, and Nanosensors for Optical Detection of Biorelevant Molecules and Ions in Aqueous Media and Biofluids. *Chem. Rev.* **2022**, *122*, 3459–3636.

(12) a) Zhang, T.; Edwards, N. Y.; Bonizzoni, M.; Anslyn, E. V. The Use of Differential Receptors to Pattern Peptide Phosphorylation. *J. Am. Chem. Soc.* **2009**, *131*, 11976–11984. (b) Wright, A. T.; Anslyn, E. V.; McDevitt, J. T. A Differential Array of Metalated Synthetic Receptors for the Analysis of Tripeptide Mixtures. *J. Am. Chem. Soc.* **2005**, *127*, 17405–17411. (c) Zamora-Olivares, D.; Kaoud, T. S.; Dalby, K. N.; Anslyn, E. V. In-Situ Generation of Differential Sensors that Fingerprint Kinases and the Cellular Response to Their Expression. *J. Am. Chem. Soc.* **2013**, *135*, 14814–14820. (d) Zeng, L.; Kaoud, T. S.; Zamora-Olivares, D.; Bohanon, A. L.; Li, Y.; Pridgen, J. R.; Ekpo, Y. E.; Zhuang, D. L.; Nye, J. R.; Telles, M.; Winkler, M.; Rivera, S.; Marini, F.; Dalby, K. N.; Anslyn, E. V. Multiplexing the Quantitation of MAP Kinase Activities Using Differential Sensing. *J. Am. Chem. Soc.* **2022**, *144*, 4017–4025.

(13) (a) Beaver, J.; Waters, M.L. Molecular Recognition of Lys and Arg Methylation. *ACS Chem. Biol.* **2016**, *11*, 643–653. (b) Daze, K. D.; Hof, F. The Cation–π Interaction at Protein–Protein Interaction Interfaces: Developing and Learning from Synthetic Mimics of Proteins That Bind Methylated Lysines. *Acc. Chem. Res.* **2013**, *46*, 937–945. (c) Minaker, S. A.; Daze, K. D.; Ma, M. C.; Hof, F. Antibody-Free Reading of the Histone Code Using a Simple Chemical Sensor Array. *J. Am. Chem. Soc.* **2012**, *134*, 11674–11680. (d) Peacor, B. C.; Ramsay, C. M.; Waters, M. L. Fluorogenic Sensor Platform for the Histone Code Using Receptors from Dynamic Combinatorial Libraries. *Chem. Sci.* **2017**, *8*, 1422–1428. (e) Harrison, E. E.; Carpenter, B. A.; St. Louis, L. E.; Mullins, A. G.; Waters, M. L. Development of "Imprint-and-Report" Dynamic Combinatorial Libraries for Differential Sensing Applications. *J. Am. Chem. Soc.* **2021**, *143*, 14845–14854.

(14) (a) Dsouza, R. N.; Hennig, A.; Nau, W. M. Supramolecular Tandem Enzyme Assays. *Chem.-Eur. J.* **2012**, *18*, 3444–3459.(b) Hennig, A.; Bakirci, H.; Nau, W. M. Label-Free Continuous Enzyme Assays with Macrocycle-Fluorescent Dye Complexes *Nat. Methods* **2007**, *4*, 629–632. (c) Nau, W. M.; Ghale, G.; Hennig, A.; Bakirci, H.; Bailey, D. M. Substrate-Selective Supramolecular Tandem Assays: Monitoring Enzyme Inhibition of Arginase and Diamine Oxidase by Fluorescent Dye Displacement from Calixarene and Cucurbituril Macrocycles *J. Am. Chem. Soc.* **2009**, *131*, 11558–11570. (d) Florea, M.; Kudithipudi, S.; Rei, A.; González-Álvarez, M. J.; Jeltsch, A.; Nau, W. M. A Fluorescence-Based Supramolecular Tandem Assay for Monitoring Lysine Methyltransferase Activity in Homogeneous Solution. *Chem. Eur. J.* **2012**, *18*, 3521–3528.

(15) Zhong, W.; Hooley, R. J. Combining Excellent Selectivity with Broad Target Scope: Biosensing with Arrayed Deep Cavitand Hosts. *Acc. Chem. Res.* **2022**, *55*, 1035–1046.

(16) (a) Liu, Y.; Perez, L.; Mettry, M.; Easley, C. J.; Hooley, R. J.; Zhong, W. Self-Aggregating Deep Cavitand Acts as a Fluorescence Displacement Sensor for Lysine Methylation. *J. Am. Chem. Soc.* **2016**, *138*, 10746–10749. (b) Liu, Y.; Perez, L.; Mettry, M.; Gill, A. D.; Byers, S. R.; Easley, C. J.; Bardeen, C. J.; Zhong, W.; Hooley, R. J. Site Selective Reading of Epigenetic Markers by a Dual-Mode Synthetic Receptor Array. *Chem. Sci.* **2017**, *8*, 3960–3970. (c) Liu, Y.; Perez, L.; Gill, A. D.; Mettry, M.; Li, L.; Wang, Y.; Hooley, R. J.; Zhong, W. Site-Selective Sensing of Histone Methylation Enzyme Activity via an Arrayed Supramolecular Tandem Assay. *J. Am. Chem. Soc.* **2017**, *139*, 10964–10967. (d) Liu, Y.; Lee, J.; Perez, L.; Gill, A. D.; Hooley, R. J.; Zhong, W. Selective Sensing of Phosphorylated Peptides and Monitoring Kinase and Phosphatase Activity with a Supramolecular Tandem Assay. *J. Am. Chem. Soc.* **2018**, *140*, 13869–13877. (e) Chen, J.; Fasihianifard, P.; Raz, A. A. P.; Hickey, B. L.; Moreno, J. L.; Chang, C.-E. A.; Hooley, R. J.; Zhong, W. Selective Recognition and Discrimination of Single Isomeric Changes in Peptide Strands with a Host:Guest Sensing Array. *Chem. Sci.* **2024**, *15*, 1885–1893.

(17) (a) Radujević, A.; Penavic, A.; Pavlović; R. Z.; Badjić, J. D.; Anzenbacher, P. Cross-Reactive Binding versus Selective Phosphate Sensing in an Imine Macrocycle Sensor. *Chem*, **2022**, *8*, 2228–2244. (b) Zyryanov, G. V.; Palacios, M. A.; Anzenbacher, P. Rational Design of a Fluorescence-Turn-On Sensor Array for Phosphates in Blood Serum. *Angew. Chem. Int. Ed.* **2007**, *46*, 7849–7852. (c) Liu, Y. C.; Peng, S.; Angelova, L.; Nau, W. M.; Hennig, A. Label-Free Fluorescent Kinase and Phosphatase Enzyme Assays with Supramolecular Host-Dye Pairs. *ChemistryOpen*, **2019**, *8*, 1350–1354. (d) Peng, S.; Barba-Bon, A.; Pan, Y.-C.; Nau, W. M.; Guo, D.-S.; Hennig, A. Phosphorylation-Responsive Membrane Transport of Peptides. *Angew. Chem. Int. Ed.* **2017**, *56*, 15742 –15745. (e) Florea, M.; Nau, W.M. Implementation of Anion-Receptor Macrocycles in Supramolecular Tandem Assays for Enzymes Involving Nucleotides as Substrates, Products, and Cofactors. *Org. Biomol. Chem.* **2010**, *8*, 1033–1039.

(18) (a) Murray, A. J. Pharmacological PKA Inhibition: All May Not Be What It Seems. *Sci. Signal.* **2008**, *1*, re4. (b) Isobe, K.; Jung, H. J.; Yang, C.-R.; Claxton, J. N.; Sandoval, P.; Burg, M. B.; Raghuram, V.; Knepper, M. A. Systems-Level Identification of PKA-Dependent Signaling in Epithelial Cells.

Proc. Natl. Acad. Sci. **2017**, *114*, E8875–E8884. (c) Shabb, J. B. Physiological Substrates of cAMP-Dependent Protein Kinase. *Chem. Rev.* **2001**, *101*, 2381–2412. (d) Ubersax, J. A.; Ferrell Jr, J. E. Mechanisms of Specificity in Protein Phosphorylation. *Nat. Rev. Mol. Cell Biol.* **2007**, *8*, 530–541. (e) Smith, F. D.; Esseltine, J. L.; Nygren, P. J.; Veesler, D.; Byrne, D. P.; Vonderach, M.; Strashnov, I.; Eyers, C. E.; Eyers, P. A.; Langeberg, L. K.; Scott, J. D. Local Protein Kinase A Action Proceeds Through Intact Holoenzymes. *Science* **2017**, *356*, 1288–1293.

(19) (a) Deretic, V. A Master Conductor for Aggregate Clearance by Autophagy. *Dev Cell.* **2010**, *18*, 694–696. (b) Ouyang, L.; Chen, Y.; Wang, Y.; Chen, Y.; Fu, A. K. Y.; Fu, W.-Y.; Yip, N. Y. p39-Associated Cdk5 Activity Regulates Dendritic Morphogenesis. *Sci. Rep.* **2020**, *10*, 18746.

(20) (a) Chen, Y.; Barkley, M. D. Toward Understanding Tryptophan Fluorescence in Proteins. *Biochemistry* **1998**, *37*, 9976–9982. (b) Ghisaidoobe, A. B. T.; Chung, S. J. Intrinsic Tryptophan Fluorescence in the Detection and Analysis of Proteins: A Focus on Förster Resonance Energy Transfer Techniques. *Int. J. Mol. Sci.* **2014**, *15*, 22518–22538. (c) Sindrewicz, P.; Li, X.; Yates, E. A.; Turnbull, J. E.; Lian, L.-Y.; Yu, L.-G. Intrinsic Tryptophan Fluorescence Spectroscopy Reliably Determines Galectin-Ligand Interactions. *Sci. Rep.* **2019**, *9*, 11851. (d) Callis, P. R. Binding Phenomena and Fluorescence Quenching. II: Photophysics of Aromatic Residues and Dependence of Fluorescence Spectra on Protein Conformation. *J. Mol. Struct.* **2014**, *1077*, 22–29.

(21) (a) Maier, J. A.; Martinez, C.; Kasavajhala, K.; Wickstrom, L.; Hauser, K. E.; Simmerling, C. ff14SB: Improving the Accuracy of Protein Side Chain and Backbone Parameters from ff99SB. *J. Chem. Theory Comput.*, **2015**, *11*, 3696–3713. (b) Miller, B. R., III; McGee, T. D., Jr.; J. M. Swails, J. M.; Homeyer, N.; Gohlke, H.; Roitberg, A. E. *MMPBSA.py*: An Efficient Program for End-State Free Energy Calculations. *J. Chem. Theory Comput.*, **2012**, *8*, 3314–3321.

(22) (a) Cortes, C.; Vapnik, V. Support-Vector Networks. *Mach. Learn.* **1995**, *20*, 273–297. (b) Ivanciuc, O. Applications of Support Vector Machines in Chemistry. *Rev. Comput. Chem.* **2007**, *23*, 291.

(23) (a) Chen, J.; Gill, A. D.; Hickey, B. L.; Gao, Z.; Cui, X.; Hooley, R. J.; Zhong, W. Machine Learning Aids Classification and Discrimination of Noncanonical DNA Folding Motifs by an Arrayed Host:Guest Sensing System. *J. Am. Chem. Soc.* **2021**, *143*, 12791–12799. (b) Chen, J.; Hickey, B. L.; Gao, Z.; Raz, A. A. P.; Hooley, R. J.; Zhong, W. Sensing Base Modifications in Non-Canonically Folded DNA with an Optimized Host:Guest Sensing Array. *ACS Sens.* **2022**, *7*, 2164–2169.

(24) Van der Maaten, L.; Hinton, G. Visualizing Data Using t-SNE. *J. Mach. Learn. Res.* **2008**, *9*, 2579–2605.

(25) (a) Devkota, A. K.; Kaoud, T. S.; Warthaka, M.; Dalby, K. N. Fluorescent Peptide Assays for Protein Kinases. *Curr. Protoc. Mol. Biol.* **2010**, *91*, 18.17.1–18.17.7. (b) O'Connor, K. L.; Mercurio, A. M. Protein Kinase A Regulates Rac and Is Required for the Growth Factor-Stimulated Migration of Carcinoma Cells. *J. Biol. Chem.* **2001**, *276*, 47895–47900.

TOC Graphic:

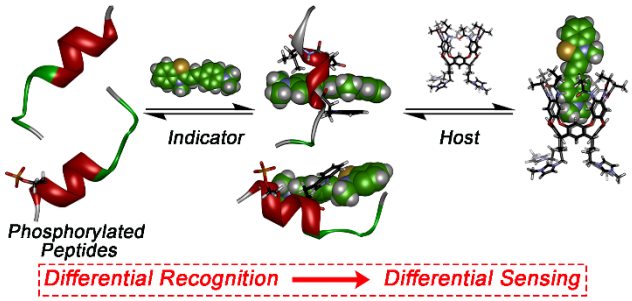
Indicator
Host
Phosphorylated Peptides
Differential Recognition
Differential Sensing